Electron-capture cross sections for Li^+ colliding on H and H_2 in the low-keV energy region

R. Cabrera-Trujillo, I. Alvarez, C. Cisneros, A. Guerrero, and J. C. Poveda
Instituto de Ciencias Físicas, Universidad Nacional Autónoma de México, Ap. Postal 48-3, Cuernavaca, Morelos, 62251, Mexico
(Received 2 July 2010; published 30 August 2010)

Absolute total and differential cross sections have been measured for neutral Li formation in single collisions of Li^+ on H_2 from 1 to 5 keV. Total cross sections were obtained by direct integration of measured differential cross sections and are in good agreement with earlier cross-sectional measurements. A comparison of the differential cross sections plotted as a function of the reduced variables $\theta \sin\theta d\sigma/d\Omega$ vs $E\theta$ is also presented with a comparison of the maximum of the curves of the present data. Theoretically, we report state to state and summed charge transfer at collision energies ranging from 0.1 to 25 keV/amu. Cross sections were calculated using a nonadiabatic time-dependent direct approach for study of ion-atom and ion-molecule interaction processes. We verify that the main electron-capture channel is in the $n = 2$ state of Li with a large probability for electron capture for impact parameters below 2 a.u. for collisions on both H and H_2 in the so-called rotational region of the collision. In the case of atomic hydrogen, the electron-capture probability into the $2s$ and $2p$ states shows an oscillating behavior that smooths out when summed. For the molecular case, we find that for projectile energies larger than 1 keV, ionization effects become important. Our results show good agreement when compared to other available experimental and theoretical data.

DOI: 10.1103/PhysRevA.82.022718 PACS number(s): 34.70.+e, 34.80.Dp, 34.80.Gs

I. INTRODUCTION

It is known that cross-sectional information on the inelastic collisions of Li^+ beams in the ground or excited state colliding with atomic and molecular species is not only of fundamental interest but also of practical importance for the diagnostics of magnetically confined fusion plasma by means of Li beams. Such collisions may result in charge transfer and energy-loss processes for which cross sections must be calculated and understood in order to fully explain the process under investigation. Recently, a proposal has been suggested for the International Thermonuclear Experimental Reactor (ITER) project in which MeV energy negatively charged deuterium ions in lithium gas charge exchange cells might produce high-energy neutral lithium atoms, which could be used for heating the ITER fusion plasma. In such a charge exchange environment, a secondary reaction involving neutral or singly positively charged lithium ions with atomic and molecular hydrogen could be expected. In this circumstance, cross sections for collision with lithium would be useful [1]. Furthermore, recent studies concerning Li beams have been carried out at the Advanced Light Source by Scully *et al.* [2] where the absolute cross section for double photoexcitation of Li^+ have been measured at high resolution. Kita and co-workers [3,4] studied the excitation mechanisms of Li^+ in collision with Ne and Ar at collision energy less than 0.5 keV. The angular distribution of the autoionized electrons have been studied by Oud *et al.* [5] in the collision of Li^+ with Ne. Experimental studies of Li^+ ions on H_2 go as far back as to those of VanEck and Kistemaker in 1960 [6]. Later Shah *et al.* [7] carried out an experimental study for Li^+ on H and H_2 in the high-energy impact region. Wutte *et al.* have compiled a data review for these systems in Ref. [8]. Theoretical studies have been carried out for Li^+ colliding on H_2 for elastic scattering and rotational excitation [9,10]. Reyes *et al.* [11] calculated the charge-transfer cross sections for the production of Li excited levels. The works of Errea *et al.* [12] and Elizaga *et al.* [13], which are based on a semiclassical eikonal and sudden approximation approach, respectively, show progress in the understanding of the electron-capture processes for Li^+ ions on hydrogen atoms and molecules.

In this paper, we present the experimental absolute differential and total cross sections for the reaction: $Li^+ + H_2 \rightarrow Li^0 + H_2^+$ from 1- to 5-keV relative energies. We also present the differential cross sections in terms of the reduced variables $\rho = \sin\theta d\sigma/d\Omega$ vs $\tau = E_p\theta$, where E_p is the projectile impact energy and θ is the scattering angle [14,15]. To complement our experimental work, a theoretical study is performed for the charge-exchange dynamics by means of a nonadiabatic time-dependent direct approach for the electron-nuclear dynamics for Li^+ ions colliding on atomic and molecular hydrogen in the ground state. We present comparisons to available theoretical and experimental data.

The paper is arranged with the following structure: In Sec. II, we provide an overview of the experimental apparatus with a discussion of the experimental procedures and errors. In Sec. III, we provide a survey of the theoretical basis and computational implementation of the method. In Sec. IV, we present our results starting with the experimental differential cross section for electron capture of Li^+ on H_2 in Sec. IV A followed by the theoretical study of the electron-capture probability in Sec. IV B. In Sec. IV C, we discuss the state-to-state and summed electron-capture cross sections. Finally, in Sec. V, we present our conclusions.

II. EXPERIMENTAL APPARATUS

The apparatus consists basically of three parts (see Fig. 1): the ion source, the scattering chamber, and the detection system. The Li^+ projectiles were produced by heating a tungsten filament covered with lithium aluminosilicate. Ions were extracted and focused by an Einzel-type lens and were directed to a Wien velocity filter in order to obtain Li^+ mass analyzed at the desired velocity.

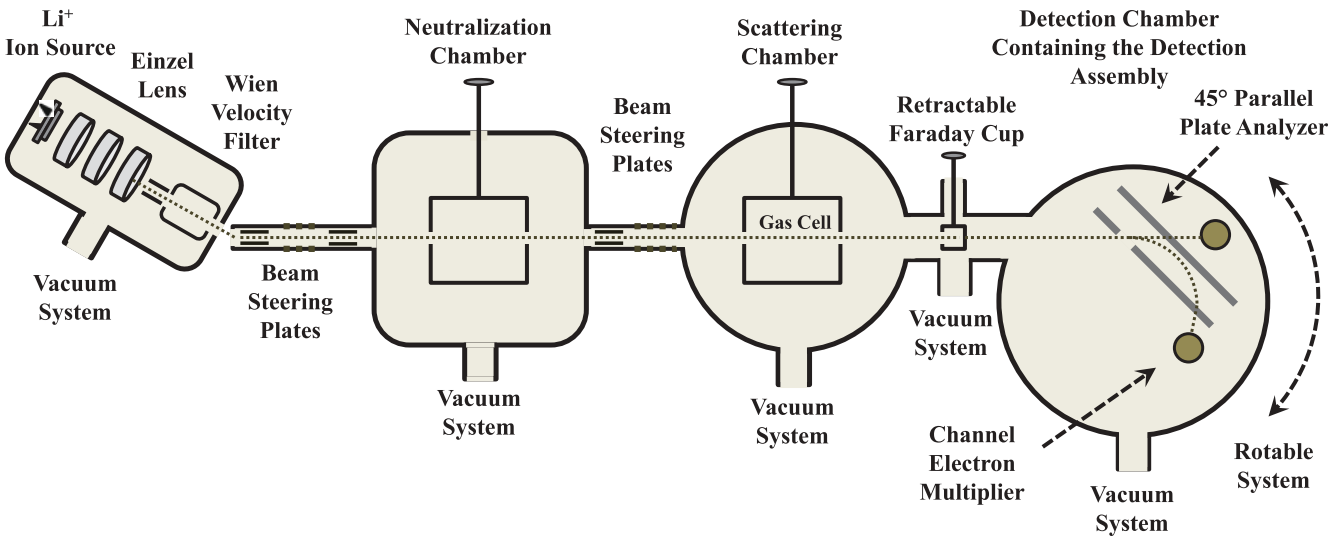

FIG. 1. (Color online) Schematics of the experimental apparatus.

The ions passed between cylindrical electrostatic deflection plates, which were used both to steer the beam and to prevent photons from the ion source reaching the detection system. The total beam current I^+ was measured by a retractable Faraday cup. The analyzed Li^+ ions entered the interaction cell, a cylinder 2.5-cm long and 2.5 cm in diameter in which the target gas pressure was measured with a calibrated capacitance manometer. The entrance of the gas cell was 1 mm in diameter, whereas the exit aperture was 3 mm in diameter. Path lengths and apertures were chosen such that the root-mean-squared angular resolution of the system was 0.1°. The detection system for the ions consists essentially of a parabolic 45° electrostatic analyzer as described by Harrower [16] with two channel electron multipliers (CEMs), one of them located in the front plate and the other in the rear plate in which an aperture was cut so that the neutrals could be monitored by a second channel electron multiplier. To measure the angular distributions, a 0.36-mm diameter pinhole was located at the entrance of the analyzer, and an orifice of 1 cm in diameter was placed in front of the CEM. The detector assembly rotates about the center of the gas cell so that the angular distributions could be obtained.

A. Experimental procedure and errors

The differential cross section was calculated from the relation,

$$\frac{d\sigma_{10}}{d\Omega} = \frac{I^0(\theta,\varphi)}{nLI^+}, \tag{1}$$

where I^+ is the number of incident Li^+ per second, n is the number of H_2 molecules per unit volume, L is the effective path length of the scattering chamber, $I^0(\theta,\varphi)$ is the number of Li^0 counts per unit solid angle per second detected at angles θ and φ, and $d\Omega$ is the solid angle subtended by the detector aperture. Here, σ_{if} is the total cross section where i refers to the initial projectile charge state, and f to the final projectile charge state. Several sources of errors are present: the effective path length, the pressure in the gas cell, the angular resolution and the integration over angle θ, the energy spread of the scattered beam, and the convolution of the detector resolution. The effective path length has been calculated up to 2.54 cm because of the gas streaming out of the apertures. The error to the path length was estimated no more than 4%. The error from the target density was estimated as a few percent. The efficiency of the CEM was corrected at each energy according to Ref. [17]. The pressure outside the collision cell was maintained in the region of 10^{-6} Torr. Increasing the pressure in these regions produced no change in the angular distributions. To eliminate slit scattering and residual gas scattering, a background distribution was measured with the collision cell evacuated. This distribution was subtracted from the scattered distribution, and the correction was always negligible. The distributions were made on both sides of the forward directions to assure us that the distributions were symmetric. The estimated root-mean-square error is 16.2%. Total cross section was derived by integrating the differential cross section over angles θ and φ. Since the scattering is symmetrical about the scattering angle φ, we have

$$\sigma_{10} = 2\pi \int_0^\pi \frac{d\sigma_{10}}{d\Omega} \sin\theta d\theta. \tag{2}$$

The absolute total total cross sections have been obtained in the energy range of 1–5 keV for the reaction $Li^+ + H_2$.

III. THEORETICAL AND COMPUTATIONAL APPROACH

A. The electron-nuclear dynamics method

We use the electron-nuclear dynamics (END) [18] theoretical approach to study the Li^+ collision with atomic and molecular hydrogen at keV energies. This is an *ab initio* explicit time-dependent theory that accounts for nonadiabatic effects. The simplest approximation, which is used in the present paper, employs a single so-called Thouless [19] determinant description of the electrons, where the spin orbitals are complex linear combinations of atomic Gaussian functions

centered on the average nuclear positions and commonly endowed with electron translation factors. Nuclei are treated as Gaussian wave packets in the narrow width limit, which is equivalent to the nuclei moving as classical particles. The dynamics takes place in a Cartesian laboratory coordinate frame, thus, translational and rotational degrees of freedom are included.

Wave-function parameters, such as average nuclear position coordinates and momenta and complex molecular orbital coefficients carry the time dependence and serve as the dynamical variables of the problem.

By applying the time-dependent variational principle to the quantum-mechanical action derived from the Hamiltonian of the system, a set of first-order differential equations in the dynamical variables is obtained, which are the equivalent of the Schrödinger equation. Integration of these coupled first-order differential equations gives, at each time step of the time evolution, the electronic wave function, and the nuclei positions and momenta.

B. Calculation details

The center-of-mass target is placed at the origin of the Cartesian laboratory coordinate system, and the projectile is placed at a distance sufficiently large so that the interaction with the target is minimal and with a momentum commensurate with the collision energy. In this particular case, we place the projectile at a distance of 200 a.u. beyond the target due to the very diffuse $n = 2$ orbitals of Li. The initial projectile velocity is set parallel to the z axis and is directed toward the target with an impact parameter b. The dynamics is stopped when the projectile has passed 200 a.u. from the target or until there is no further change in the charge-transfer probability due to interactions of the projectile and target electronic cloud. For the case of a molecular target, we specify its orientation by angles α and β as shown in Fig. 2.

The initial conditions include the determination of a proper electronic state of the target and projectile system. A proper choice of basis set is crucial in this method. We use Gaussian basis sets centered on the average nuclear positions. From these, we form linear combinations of atomic orbitals, which become the molecular orbitals of the system. For the Li ion projectile, we use a $[6s3p/2s1p]$ basis set from Hehre *et al.* [20], augmented by two s and one p even-tempered diffuse orbitals to allow for low-lying excited states of the projectile. For the atomic and molecular hydrogen target we obtain a self-consistent field ground state by means of a $[5s2p/3s2p]$ basis set from Dunning [21], augmented by two s and two p even-tempered diffuse orbitals to reproduce the low excited states. The exponents used in our calculations for the basis set have already been reported in a previous study [22] regarding these two atoms.

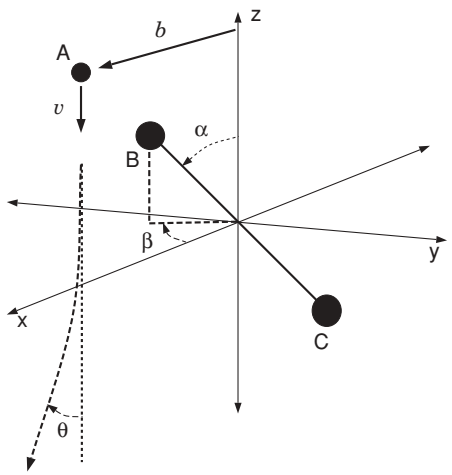

FIG. 2. Schematic of the space-fixed molecular coordinate frame that represents the projectile and target orientations.

A number of END trajectories are run with different impact parameters ranging from 0.0 a.u. up to 20 a.u. We consider three ranges of impact parameter; (1) the close interaction region that goes from 0.0 up to 6.0 a.u. in steps of 0.1 a.u.; (2) the intermediate region covers the range from 6 to 10 a.u. in steps of 0.5 a.u.; (3) and the long-range interaction region covers the impact parameters from 10 to 20 a.u. in steps of 1.0 a.u. This yields trajectories for a total of 79 impact parameters per projectile energy. The probabilities for electron capture are thus calculated from these trajectories to obtain charge-transfer probabilities and cross sections.

The electron-capture probability is obtained by projecting the final evolved electronic wave function on a particular electronic state of the projectile, expressed in terms of the projectile basis set. The probability for finding the electron in that final state Ψ_f is thus given by $P_f(b) = |\langle \Psi_f | \Psi_j \rangle|^2$ where Ψ_j is the electronic state wave function at the end of the dynamics as a result of being initially in the j state. Ψ_f is a particular stationary electronic state on the projectile we are interested in (e.g., the $2s$ state of lithium).

Finally, the electron-capture cross section into a final state f of the projectile is calculated from the electron-capture probability as

$$\sigma_{10}^{f}(E_p) = 2\pi \int_0^\infty b P_f(b, E_p)\, db. \tag{3}$$

In the case of atomic projectiles, as in this case, we need to consider the initial orientations of only the target. For homonuclear diatomic molecules, we consider three orientations of the target with respect to the direction of the incoming beam. These orientations yield a coarse set of grid points for rotational averaging. The three basic target orientations place the molecular bond along the x, y, and z axes. We will label these three orientations as $(\alpha = 0, \beta = 0)$, for the molecular bond aligned parallel to the incoming beam; $(\alpha = \pi/2, \beta = 0)$, for the molecular bond perpendicular to the beam, but with the impact parameter measured along the bond length; and $(\alpha = \pi/2, \beta = \pi/2)$ for the molecular bond perpendicular to the beam, as well as the impact parameter [see Fig. 2]. The average over the orientation is calculated by assuming that each of these orientations has the same probability in the gas cell, thus, any averaged property g_{avg} is obtained as

$$g_{\text{avg}} = [g(\alpha = 0, \beta = 0) + g(\alpha = \pi/2, \beta = 0) + g(\alpha = \pi/2, \beta = \pi/2)]/3. \tag{4}$$

IV. RESULTS

A. Electron-capture differential cross section

The experimental data are presented in Table I where we give them in the so-called reduced variables $\tau = E_p\theta$ where E_p is the projectile impact energy and θ is the scattering angle. The reduced cross section is the quantity $\rho = \theta \sin\theta d\sigma_{10}/d\Omega$ [14,15]. The reduced cross sections presented are the sum of all the contributions to produce Li^0. The reason for the choice of these variables is shown in Fig. 3 where we plot the reduced cross section $\theta \sin\theta d\sigma_{10}/d\Omega$ as a function of the reduced variables $E_p\theta$. Thus, in the small-angle forward scattering, a scaling law is present, characteristic of the interaction at large impact parameters [14,15]. We observe that the data have a maximum for $E_p\theta$ between 2° and 4° keV. The experimental data start to spread for large scattering angles showing differences in the atomic interaction for small impact parameters.

TABLE I. Experimental data for the reduced differential cross section for electron capture as a function of the reduced variable $E_p\theta$. The projectile energy E_p is given in keV and the scattering angle θ in degrees. At the bottom of the table, we provide the total electron-capture cross sections for $Li^+ + H_2$ obtained by Eq. (2). The units are in 10^{-16} cm^2.

$\tau = E_p\theta$	$\rho(E_p) = \theta \sin\theta d\sigma_{10}/d\Omega$					
(keV deg)	1.0	1.5	2.0	3.0	4.0	5.0
0.25	0.0279	0.0559	0.0782	0.188	–	–
0.55	0.0651	0.111	0.144	0.278	0.354	0.442
0.85	0.115	0.201	0.240	0.421	0.509	0.583
1.15	0.172	0.304	0.345	0.588	0.704	0.798
1.45	0.255	0.412	0.483	0.772	0.926	1.06
1.75	0.358	0.552	0.632	0.979	1.19	1.35
2.05	0.459	0.705	0.781	1.25	1.49	1.67
2.35	0.529	0.874	0.967	1.51	1.78	1.94
2.65	0.499	1.05	1.15	1.71	2.04	2.16
2.95	0.492	1.15	1.25	1.83	2.16	2.29
3.25	–	1.16	1.32	1.88	2.19	2.31
3.55	–	1.08	1.40	1.88	2.14	2.27
3.85	–	1.03	1.42	1.87	2.06	2.17
4.15	–	0.983	1.31	1.81	1.96	2.06
4.45	–	0.951	1.24	1.73	1.86	1.95
4.75	–	0.970	1.19	1.68	1.76	1.82
5.05	–	0.969	1.09	1.65	1.65	1.74
5.35	–	0.915	0.983	1.68	1.58	1.67
5.65	–	0.882	0.894	1.69	1.50	1.58
5.95	–	–	0.836	1.55	1.44	1.46
6.25	–	–	0.791	1.35	1.36	1.35
6.55	–	–	0.759	1.25	1.36	1.28
6.85	–	–	0.740	1.20	1.36	1.21
7.15	–	–	0.700	1.12	1.41	1.15
7.45	–	–	–	1.07	1.39	1.11
7.75	–	–	–	0.974	1.32	1.08
8.05	–	–	–	0.823	1.20	1.06
8.35	–	–	–	0.723	1.10	1.04
8.65	–	–	–	0.677	1.06	1.03
8.95	–	–	–	0.650	1.00	1.00
9.25	–	–	–	0.612	0.982	0.961
9.55	–	–	–	0.578	0.957	0.900
9.85	–	–	–	0.574	0.926	0.864
10.1	–	–	–	0.579	0.885	0.848
10.4	–	–	–	0.611	0.769	0.829
10.7	–	–	–	0.612	0.657	0.805
11.0	–	–	–	–	0.585	0.781
11.3	–	–	–	–	–	0.767
11.6	–	–	–	–	–	0.765
11.9	–	–	–	–	–	0.770
σ	0.121	0.205	0.223	0.379	0.446	0.481
	±0.019	±0.033	±0.036	±0.06	±0.07	±0.08

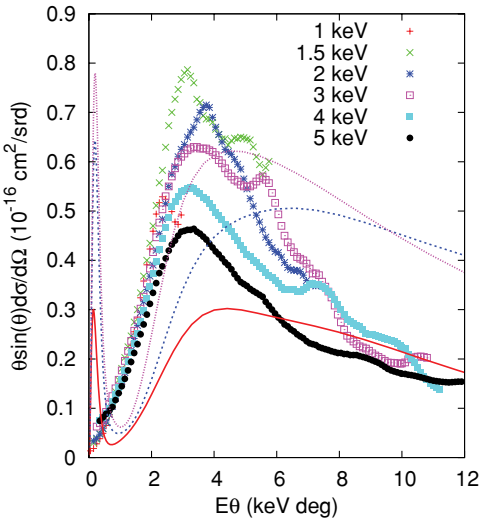

FIG. 3. (Color online) Reduced electron-capture differential cross section to form Li^0 when Li^+ collide with molecular hydrogen as a function of the reduced variable $E_p\theta$. Our theoretical results are represented by lines: solid line, 1 keV; dashed line, 2 keV; dotted line, 3 keV.

In the same figure, we show our theoretical results obtained by means of a semiclassical correction due to Schiff [23] and implemented by Cabrera-Trujillo *et al.* [24] that includes the rainbow and glory angle scatterings. The first peak is located around $E_p\theta \sim 0.1$ corresponding to the forward scattering (including glory angle). The second peak is located around $E_p\theta \sim 4$ in reasonable agreement with the experimental data. The discrepancy could be due to the coarse orientational grid used for the molecular target.

B. Electron-capture probability

$Li^+ + H$: In Fig. 4, we show the total electron-capture probability to form Li^0 when Li^+ collides on atomic hydrogen as a function of the projectile impact parameter and collision energy as obtained by our theoretical approach. The electron-capture probability decreases for lower projectile energies with its large contribution in the small impact parameter region. Furthermore, it presents an ascending ridge around $b \sim 0.5$ a.u. from the low projectile energy region with a peak at $E_p \sim 5$ keV/amu. In the higher-energy region, there is another ridge around $b \sim 2$ a.u. Interestingly, the larger contribution to the electron-capture cross section arises from impact parameter in the small impact parameter region ($b < 2.0$ a.u.).

In Fig. 5, we show the total probability for electron capture for Li^+ colliding on atomic hydrogen as a

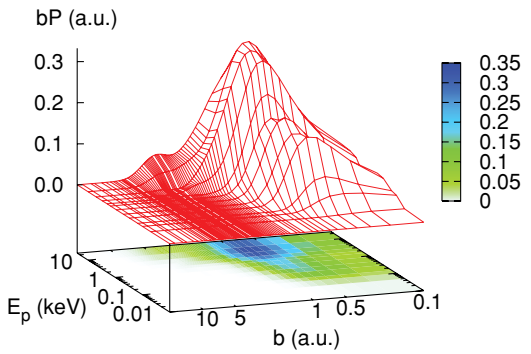

FIG. 4. (Color online) Total electron-capture probability to form Li^0 when Li^+ collides with atomic hydrogen as a function of the projectile impact parameter and energy.

function of the impact parameter for a collision energy of 1 keV/amu and compare with the theoretical results of Errea *et al.* [12] obtained by their semiclassical eikonal treatment with nuclear straight-line trajectories. From these results, we notice that although the maxima and trend are similar, our results are lower by 20% when compared to their results. The difference seemingly is due to the way the projectile trajectories are treated in both approaches. This difference will appear in the total electron-capture cross section.

$Li^+ + H_2$: In Fig. 6, we show the total averaged over the orientations electron-capture probability to form Li^0 when Li^+ collides on molecular hydrogen as a function of the projectile impact parameter and collision energy. At a glance, it looks similar to the atomic hydrogen case (Fig. 4).The electron-capture probability decreases for lower projectile energies with its larger contribution arising in the small impact parameter region at the high-energy region. Furthermore, it presents a ridge around $b \sim 0.5$ a.u. from the low projectile energy region, but there is no peak at $E_p \sim 5$ keV/amu as in the atomic case, but it keeps increasing for higher energies. The ridge around $b \sim 2$ a.u., present in

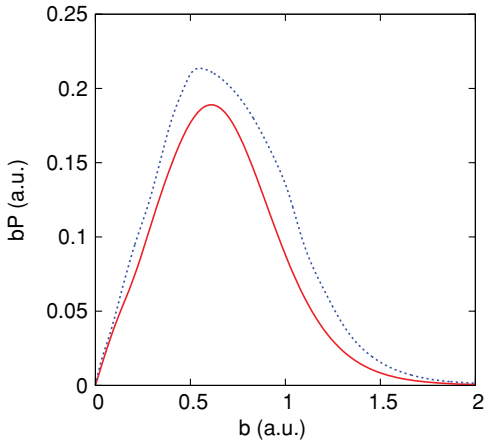

FIG. 5. (Color online) Total electron-capture probability to form Li^0 when Li^+ collide with atomic hydrogen as a function of the projectile impact parameter. Our theoretical results (solid line) are compared to Errea *et al.* for a collision energy of 1 keV [12] (short-dashed line).

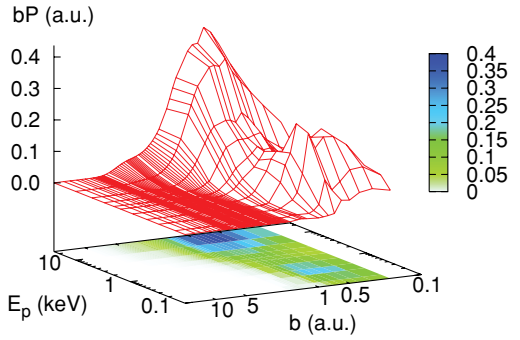

FIG. 6. (Color online) Total averaged over the target orientations electron-capture probability to form Li^0 when Li^+ collide with molecular hydrogen as a function of the projectile impact parameter and energy.

the atomic case, is not that obvious for the molecular case, although it can be discerned. Furthermore, the ridge is less smooth than the atomic case. The reason is that the orientation ($\alpha = 90, \beta = 0$) where the impact parameter runs over the molecular bond produces an increase in the capture probability around $b \sim 0.7$ a.u. that coincides with the head-on collision with the hydrogen target on the H_2 molecule. Also note that the probability is almost twice that of the atomic case, since now we have a target with α- and β-spin electrons with the same probability of being captured in this approach.

C. Electron-capture cross section

$Li^+ + H$: In Fig. 7, we show the total (summed) electron-capture cross section σ_{10} for Li^+ ions colliding with atomic hydrogen as a function of the projectile energy as obtained by our theoretical approach. In the same figure, we compare our

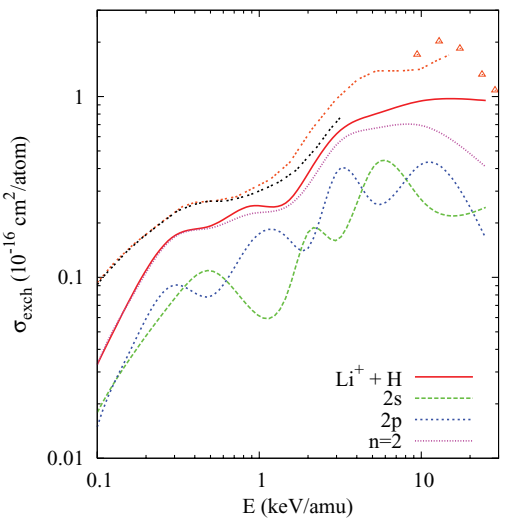

FIG. 7. (Color online) Total charge-transfer cross section for Li^+ colliding with atomic hydrogen as a function of the projectile energy. Solid-thick line, this paper for the total-capture cross section; long-dashed line, capture into the Li($2s$); short-dashed line, capture into Li($2p$); dotted line, capture into the $n = 2$ state of Li; triple-dotted line, theoretical results of Errea *et al.* [12] for the total electron-capture cross section and double-dotted line for the capture into the $n = 2$ state of Li. Experimental data, open triangles; Shah *et al.* [7] for H.

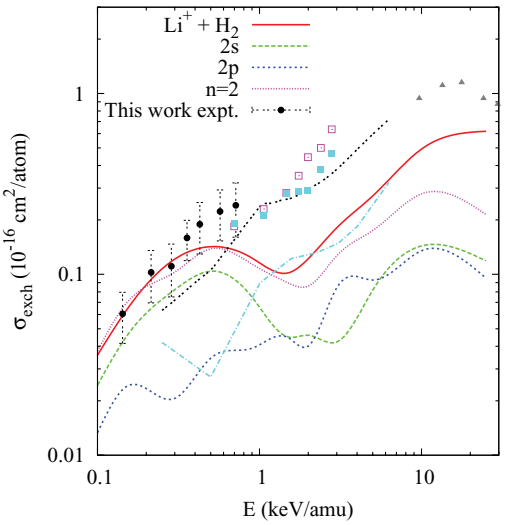

FIG. 8. (Color online) Total charge-transfer cross section per target atom for Li^+ colliding with molecular hydrogen as a function of the projectile energy. Solid-thick line, this paper for the total-capture cross section; long-dashed line, capture into the Li($2s$); short-dashed line, capture into Li($2p$); dotted line, capture into the $n = 2$ state of Li; double-dotted line, theoretical results of Elizaga *et al.* [13] for the electron-capture cross section in the $2l$ state and dot-dashed line for the capture into the $2s$ state of Li. Full circles, our experimental results; open squares, Wutte *et al.* [8]; full squares, VanEck and Kistemaker [6]; full triangles, Shah *et al.* [7].

theoretical results to the experimental data of Shah *et al.* [7] in the high-energy region.

In the same figure (Fig. 7), we show the electron-capture probability into the $2s$, $2p$, and the summed $n = 2$ excited state, which is the main capture channel for this process for collision energy below 5 keV/amu. The first characteristic is that for projectile energies above 0.5 keV/amu; the capture into the $2s$ and $2p$ states oscillates and alternates, however, their sum (the $n = 2$ contribution) presents a smooth behavior. For projectile energies above 5 keV/amu, higher excited states and the ionization channel start to contribute and become important. For projectile energies larger than 10 keV/amu, the ionization channel completely opens. In the same figure, we also show the theoretical results of Errea *et al.* [12] for the total (dot-short-dashed line) and the electron capture into the $n = 2$ (double-dotted line), which are obtained by means of a semiclassical approach based on straight trajectories. As observed, their results are around 20% higher than our theoretical results.

$Li^+ + H_2$: In Fig. 8, we show the theoretical and experimental total (summed) averaged over the target orientations electron-capture cross section σ_{10} for Li^+ ions colliding with molecular hydrogen as a function of the projectile energy. We compare our results with the experimental data of Wutte *et al.* [8], VanEck and Kistemaker [6], and those of Shah *et al.* [7]. Also, we compare with the theoretical results of Elizaga *et al.* [13] for the $2l$ and $2s$ contributions on Li obtained by means of a sudden approximation approach. The $2l$ results of Elizaga *et al.* closely follow the experimental data for collision energies larger than 1 keV/amu but fall below our experimental data at lower collision energy. On the contrary, our theoretical results closely follow the experimental data for collision energies below 1 keV/amu and stay below the experimental data for higher collision energies.

In the same figure, we show the electron-capture probability into the $2s$, $2p$, and the summed $n = 2$ excited state averaged over the target excitations. We observe that in the low-to-intermediate energies, $n = 2$ is the main capture channel for this process. Comparing with the atomic case, the capture into the $2s$ and $2p$ states does not show the oscillating and alternating behavior. Our $n = 2$ capture cross section falls below by a factor of 2 for collision energies larger than 1 keV/amu when compared to the results of Elizaga *et al.* and the experimental results. The inverse occurs for collision energies below 1 keV/amu. The reason being the opening of the ionization channel and the failure of the single determinant to describe molecular fragmentation and ionization simultaneously.

V. CONCLUSIONS

In this paper, we have presented the differential and total electron-capture cross section for Li^+ ions colliding on molecular hydrogen obtained experimentally in our laboratory and complement our study by means of state-to-state and total electron-capture cross sections by means of a nonadiabatic fully coupled electron-nuclear dynamics study in the low-energy region for both atomic and molecular hydrogen targets. We verify that the main electron-capture channel is into the $n = 2$ state of lithium. Our experimental and theoretical results show good agreement with existing models and good accord with experimental data in the low collision energy region. For the molecular case, it is necessary that the proper inclusion of the ionization channel and a multireference state description of the dynamics fully account for the molecular fragmentation and ionization at high collision energies. We hope this work will motivate more experimental and theoretical studies for lithium ions colliding on atomic and molecular hydrogen.

ACKNOWLEDGMENTS

This work has been partially supported by CONACYT Project No. 82521 to I.A. and C.C. and by DGAPA-UNAM through Projects No. IN-108-009 to C.C., No. IN-107-310 to I.A., and No. IN-107-108 to R.C.T.

[1] L. R. Grisham, Phys. Plasmas **14**, 102509 (2007).
[2] S. W. J. Scully *et al.*, J. Phys.: Conf. Ser. **58**, 387 (2007).
[3] S. Kita and N. Shimakura, Phys. Rev. A **55**, 3504 (1997).
[4] S. Kita, S. Gotoh, N. Shimakura, and S. Koseki, Phys. Rev. A **62**, 032704 (2000).
[5] M. Oud, S. F. te Pas, W. B. Westerveld, and A. Niehaus, J. Phys. B **26**, 1641 (1993).
[6] J. VanEck and J. Kistemaker, Physica **26**, 629 (1960).
[7] M. B. Shah, T. V. Goffe, and H. B. Gilbody, J. Phys. B **11**, L233 (1978).

[8] D. Wutte, R. K. Janev, F. Aumayr, M. Schneider, J. Schweinzer, J. J. Smith, and H. P. Winter, At. Data Nucl. Data Tables **65**, 155 (1997).
[9] R. Schinke, Chem. Phys. **34**, 65 (1978).
[10] K. J. McCann and M. R. Flannery, J. Chem. Phys. **69**, 5275 (1978).
[11] A. Reyes, D. Micha, and K. Runge, Chem. Phys. Lett. **363**, 441 (2002).
[12] L. F. Errea, F. Guzmán, L. Méndez, B. Pons, and A. Riera, Phys. Rev. A **77**, 012706 (2008).
[13] D. Elizaga, L. F. Errea, J. D. Gorfinkiel, L. Méndez, A. Macías, A. Riera, and A. Rojas, J. Phys. B **33**, 2037 (2000).
[14] C. Lehmann and G. Leibfried, Z. Physik **172**, 465 (1963).
[15] F. T. Smith, R. P. Marchi, and K. G. Dedrick, Phys. Rev. **150**, 79 (1966).
[16] G. A. Harrower, Rev. Sci. Instrum. **26**, 850 (1955).
[17] D. H. Crandall, J. A. Ray, and C. Cisneros, Rev. Sci. Instrum. **46**, 562 (1975).
[18] E. Deumens, A. Diz, R. Longo, and Y. Öhrn, Rev. Mod. Phys. **66**, 917 (1994).
[19] D. J. Thouless, Nucl. Phys. **21**, 225 (1960).
[20] W. J. Hehre, R. F. Stewart, and J. A. Pople, J. Chem. Phys. **51**, 2657 (1969).
[21] T. H. Dunning, J. Chem. Phys. **90**, 1007 (1989).
[22] R. Cabrera-Trujillo, J. R. Sabin, E. Deumens, and Y. Öhrn, Phys. Rev. A **78**, 012707 (2008).
[23] L. I. Schiff, Phys. Rev. **103**, 443 (1956).
[24] R. Cabrera-Trujillo, J. R. Sabin, Y. Öhrn, and E. Deumens, Phys. Rev. A **61**, 032719 (2000).